SPIV investigations of correlation between streamwise vorticity and velocity in the wake of a vortex generator in a boundary layer

Velte, Clara Marika; Okulov, Valery; Hansen, Martin Otto Laver

Published in:
Proceedings of 10th International Symposium on Particle Image Velocimetry - PIV13

Publication date:
2013

Document Version
Peer reviewed version

10TH INTERNATIONAL SYMPOSIUM ON PARTICLE IMAGE VELOCIMETRY - PIV13
Delft, The Netherlands, July 1-3, 2013

SPIV investigations of correlation between streamwise vorticity and velocity in the wake of a vortex generator in a boundary layer

Clara M. Velte[1], Valery L. Okulov[2] and Martin O.L. Hansen[2]

[1] Department of Mechanical Engineering, Technical University of Denmark, Nils Koppels Allé B403, 2800 Kgs. Lyngby, Denmark, cmve@dtu.dk

[2] Department of Wind Energy, Technical University of Denmark, Nils Koppels Allé B403, 2800 Kgs. Lyngby, Denmark

ABSTRACT

The current work describes the experimental parametric study of streamwise vortices generated in a boundary layer by a rectangular vane (commonly named vortex generator) mounted perpendicularly to the wall and at an angle to the oncoming flow. Stereoscopic Particle Image Velocimetry measurements have been conducted in cross-planes to obtain a full picture of the wake for each measured case. It is observed that this seemingly simple configuration produces a complicated vortex system consisting of 4 vortices: the tip vortex, a horseshoe vortex system consisting of two sleeves and a secondary vortex generated by the interaction between the tip vortex and the wall. Depending on the height and angle of the vane, some structures are enhanced and others are suppressed. Comparing the corresponding vorticity and velocity fields, a strong correlation between the two is found. Stream-wise vorticity induced velocity with the observed strong correlation found is not at all evident. This has previously been shown to be true for the primary (tip) vortex, but not for the remaining secondary structures.

Introduction

In recent years, the use of vortex generators (VGs) in aerodynamics has become a widely used method for suppressing the separation of a boundary layer from various surfaces, including airfoils, turbine blades, nozzles, diffusers, etc. The use of VGs for preventing flow separation in diffusers was originally proposed in 1974 by Taylor [1]. A VG typically represents a short vane arranged perpendicular to the surface, at a certain angle of attack relative to the oncoming flow, so that the circulation flow past the VG forms a longitudinal tip vortex. In the presence of a VG, the flow separation is significantly delayed or even eliminated due to redistribution of the longitudinal momentum of the moving medium. This approach to form a large scale vortex motion in the boundary layer for re-energizing the flow is one example of passive control of flow separation. The positive effect was studied and confirmed for various VG configurations and related vortex flow regimes. However, the vortex structures induced in the VG wake are still insufficiently studied and identified. For more effective simulation and control of VG-induced vortex flows, this gap must evidently be closed.

We have studied the flow structures downstream of an elementary VG representing a simple rectangular flat plate by the method of Stereoscopic Particle Image Velocimetry (SPIV) [2] and observed, in addition to the primary longitudinal tip vortex, some additional secondary vortex structures in several regimes. The presence of secondary vortices leads to perturbations and deformations of the primary vortex [2] and influences its position [3, 4]. Therefore, it was expedient to study the vortex structure behind the VG in more detail for a wider range of flow regime parameters.

The present investigation was originally aimed at detecting and explaining the appearance of stable multi-vortex structures in the wake of a rectangular VG or small vane in a near-wall boundary layer [5]. The resulting wakes, which were mapped in regimes, showed, in themselves, interesting results. However, when comparing the stream-wise velocity and vorticity, they displayed quite similar distributions and are hence connected. The current work aims to show the existence of this correlation and discuss the implications of this result.

1. Method

The experiments were carried out in a low Reynolds number closed loop wind tunnel with an 8:1 contraction ratio and a test section of cross-sectional area 300×600 mm with length 2 m. The test section had optical access through the top and bottom walls as well as through the sidewall opposite to the wall with the attached vortex generator. The wind tunnel speed was obtained by measuring the pressure drop across an orifice plate. The turbulence intensity at the inlet from laser doppler anemometry (LDA) measurements has been found to be 13%. The boundary layer thickness at the position of the vortex generator has been estimated from LDA measurements to be approximately $\delta_{VG}=25$ mm.

A single rectangular vane was mounted on one of the test section walls with a variable angle of attack to the oncoming flow. The vortex generator was positioned on a vertical wall in the center of the test section with its trailing edge 750 mm downstream of the inlet grid when it is at zero angle to the mean flow. In order to easily and accurately alter the device angle, the vortex generator was attached to a pin which could be accessed from outside the test section through a hole in the test section wall. This pin was in turn attached to a

pointer arm placed over a protractor indicating the relative angle of the actuator to the mean flow direction. The protractor had a radius of 200 mm and grading for integer values of each degree.

Stereoscopic PIV measurements were performed in cross planes 10 vane heights (h) downstream of the trailing edge of a single rectangular vane in a first round. The vane had a thickness of about 1 mm. In order to avoid reflections from the wall and the vortex generator within the wavelength band of the camera filters, these areas were treated with a fluorescent dye, Rhodamine 6G, mixed with matt varnish to obtain a smooth surface and to ensure that the dye stayed attached. The cameras were in turn equipped with band-pass filters designed to only pass light with wavelengths close to that of the laser light so that unwanted reflections were not recorded by the cameras. The angle of attack relative to the oncoming flow direction was varied from 9° to 54° with increments of 3°. In addition, the VG height was varied from 5 to 25 mm with increments of 5 mm. The vane length (l) was always set to twice its height ($l = 2$h). With a free-stream velocity of $U_\infty = 1$ m/s and a VG height of between 5-25 mm, the Reynolds number varied between about 300 and 1 700.

The SPIV equipment was mounted on a rigid stand and included a double cavity NewWave Solo 120XT Nd-YAG laser (wavelength 532 nm) capable of delivering light pulses of 120 mJ. The pulse width, i.e. the duration of each illumination pulse, was 10 ns. The light-sheet thickness at the measurement position was 2 mm and was created using a combination of a spherical convex and a cylindrical concave lens. The equipment also included two Dantec Dynamics HiSense MkII cameras (1344×1024 pixels) equipped with 60 mm lenses. Both cameras were mounted on Scheimpflug angle adjustable mountings. The seeding, consisting of DEHS (diethyl-hexyl-sebacin-esther) droplets with a diameter of 2.3 μm, was added to the flow downstream of the test section in the closed-circuit wind tunnel in order to facilitate a homogeneous distribution of the particles before they enter the test section. The two cameras were placed in the forward scattering direction. The angle of each respective camera to the laser sheet was 45°. The f-numbers of the cameras were set to 2.8, yielding a depth of field which is small but sufficient to cover the thickness of the laser sheet and keeping all illuminated particles in focus while still attaining sufficient scattered light from the tracer particles. A calibration target was aligned with the laser sheet. This target had a well-defined pattern, which could be registered by the two cameras to obtain the geometrical information required for reconstructing the velocity vectors received from each camera to obtain a full description of all three velocity components in the plane. Calibration images were recorded with both cameras at five well-defined stream-wise positions throughout the depth of the laser sheet in order to capture the out-of-plane component in the reconstructed coordinate system of the measurement plane under consideration. A linear transform was applied to these images for each camera to perform the reconstruction. This procedure was executed both previous to and after the conduction of the measurements to ensure that no drift had occurred. The images were processed using Dantec DynamicStudio software version 2.0. Adaptive correlation was applied using refinement with an interrogation area size of 32×32 pixels. Local median validation was used in the immediate vicinity of each interrogation area to remove spurious vectors between each refinement step. The overlap between interrogation areas was 50%. For each measurement position, 500 realizations were acquired. The recording of image maps was done with an acquisition rate of 1.0 Hz, ensuring statistically independent realizations based on the convection velocity $U_\infty = 1.0\,\mathrm{ms}^{-1}$ and the mesh size $d = 0.039$ m, yielding a time scale of $t = d/U_\infty = 0.039$ s. The velocity vector maps contain 73×61 vectors. The linear dimensions of the interrogation areas (x,y)=(1.55,1.04) mm can be compared to the Taylor microscale and the Kolmogorov length scale estimated to $\lambda_f \approx 9$ mm and $\eta \approx 0.5$ mm from LDA measurements [6].

After analysis of the initial measurements, a second campaign was initiated where the most interesting cases were investigated more in-depth by mapping the downstream evolution of the wake in a number of planes covering both the near and the far wake. In the current study, measurements at positions 3h and 10h downstream of the trailing edge have been utilized. The experimental setup represented a slightly modified system described elsewhere [2] and further details can also be found in [5].

2. Results

2.1 Wake regimes

From water channel visualizations, the basic vortex structures were identified and subsequently schematically depicted in Figure 1 (c.f. [5]). A circular flow past the plate oriented at the attack angle results in separation of the primary vane tip vortex *P* from the upper edge of the plate. In addition, a pressure distribution around the leading edge creates a weaker horseshoe-like vortex with two arms occurring on opposite sides of the VG plate and passing downstream from the excess-pressure (H_P) and -suction (H_S) sides of the plate. The existence of these clearly pronounced horseshoe vortices was also observed in the flow past fixed ends of blades in axial turbines [5], where these vortices form a system of interblade forces. In the case of VGs, the H_P and H_S horseshoe vortices are strongly influenced by the primary tip vortex and their behavior is thus somewhat different from that in the axial turbines.

At an early stage, the primary vortex *P* sweeps the H_S horseshoe vortex underneath itself and drives it to the side of H_P vortex, which develops independently of the (P, H_S) pair. It was established that the horseshoe vortex does not appears in all flow regimes. The formation of this vortex depends on the angle of attack and the relative VG height compared to the boundary layer thickness. For certain values of these parameters, perturbations introduced by the vane are insufficiently large and the resulting side arms cannot be identified as vortices with individual cores and only appear as vorticity clouds on the surface. Thus, two typical configurations of principal vortex structures consisting of one (P) or three (P, H_S, H_P) can appear in the wake flow downstream of the VG blade.

In addition to the principal vortex structure described above, a secondary vortex system *S* can appear downstream of the VG as a result of the interaction of the primary tip vortex with the boundary layer. A physical mechanism of this process was described long ago [7], while imaging and identification of the primary and secondary vorticity was reported quite recently [4]. In the regimes where only the primary longitudinal vortex is well distinguished, the formation of a secondary vortex is also well illustrated by the results of our SPIV measurements [2] in the wind tunnel, see Figure 2. As the angle of attack is increased, the intensity of the tip vortex grows and its action upon the boundary layer increases. As a result, the region of vorticity concentration in the boundary layer on the right grows and eventually pinches off and forms an additional discrete vortex, *D*. This result agrees with the description of the mechanism of a secondary vortex structure in [7].

Thus, the vortex structure downstream of the VG can represent various numbers and combinations of the primary and secondary vortex structures. Taking into account the complex dynamics of the flow, with the possible interaction and merger of vortices with each other, it is impossible to predict their number and mutual arrangement. For this reason, we have carried out a complete parametric investigation of the development of multi-vortex regimes in a wake past a model VG. The flow regimes were changed by varying the geometric parameters of the VG, including the attack angle β and height h/δ of the vane, where δ is the local boundary layer thickness. As a result, three stable regimes have been established for the vortex system downstream of the VG. Figure 3a shows examples of the distribution of the axial component of vorticity in these regimes with increasing number of vortices in the wake. Figure 3b presents a map of the possible regimes of flow past the VG.

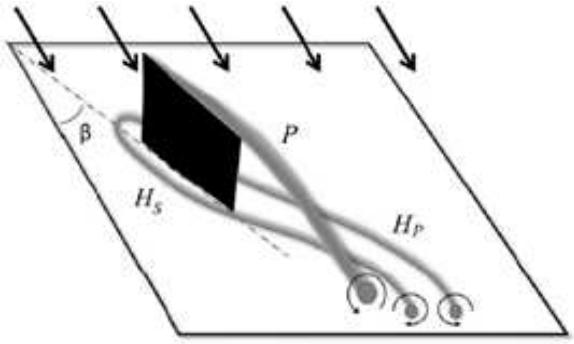

Figure 1: Sketch of vortex structures observed around a wall-mounted vane.

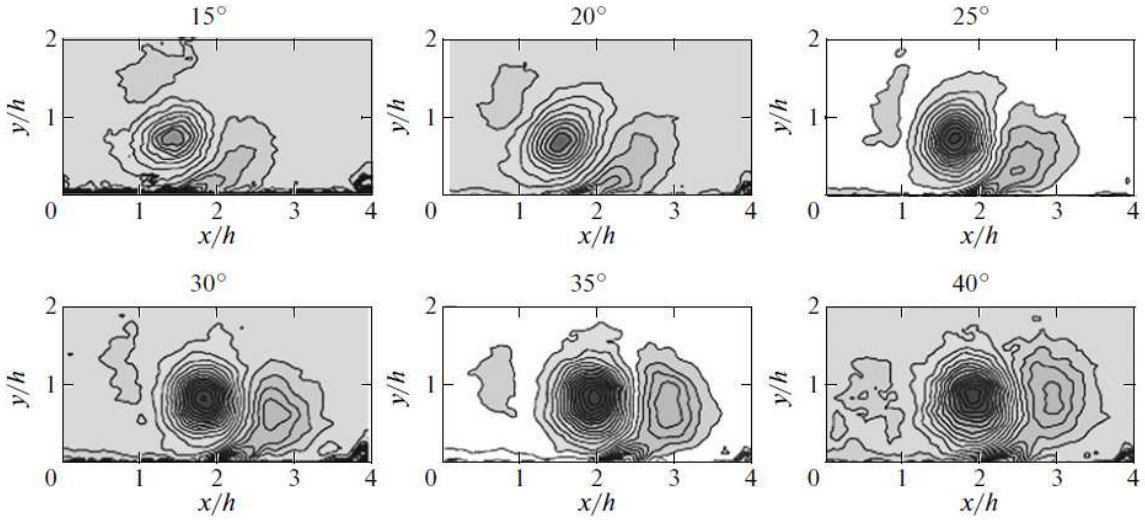

Figure 2: Generation of secondary vortex structures by a VG with increasing angle of attack.

2.2 Connection between stream-wise velocity and vorticity

In the process of the previous investigations, the stream-wise velocity and vorticity fields were investigated. It was observed, both in the near wake and in the stable far wake of the vortex generator, that these display a clear coupling. Figures 4 and 5, display the stream-wise vorticity (left column) and corresponding stream-wise velocity (right column) fields for vane angles 21°, 33°, 48° and 54° at 3*h* and 10*h* downstream of the vane trailing edge, respectively. At both positions, the two quantities are seen to be correlated. This was previously know to be true for the primary vortex [2], but not for the secondary vortex structures.

3. Summary and conclusions

The emergence of secondary structures is observed to be highly dependent on the geometric attributes of the vortex generator, and can result in a range of various far wake states. However, independently of which state is considered, the stream-wise velocity and vorticity fields display a directly visible correlation for all flow structures, including the secondary ones. The direct relation between these variables was previously known to exist for the primary vortex, but not for the secondary structures. This is an important result for understanding the vortex generator wake, due to the coupling between the secondary and the primary velocity components. This knowledge can be implemented in models of the wake of VGs, e.g., in boundary layers, but is also interesting from a more fundamental point of view to describe and control vortical motions behind VGs.

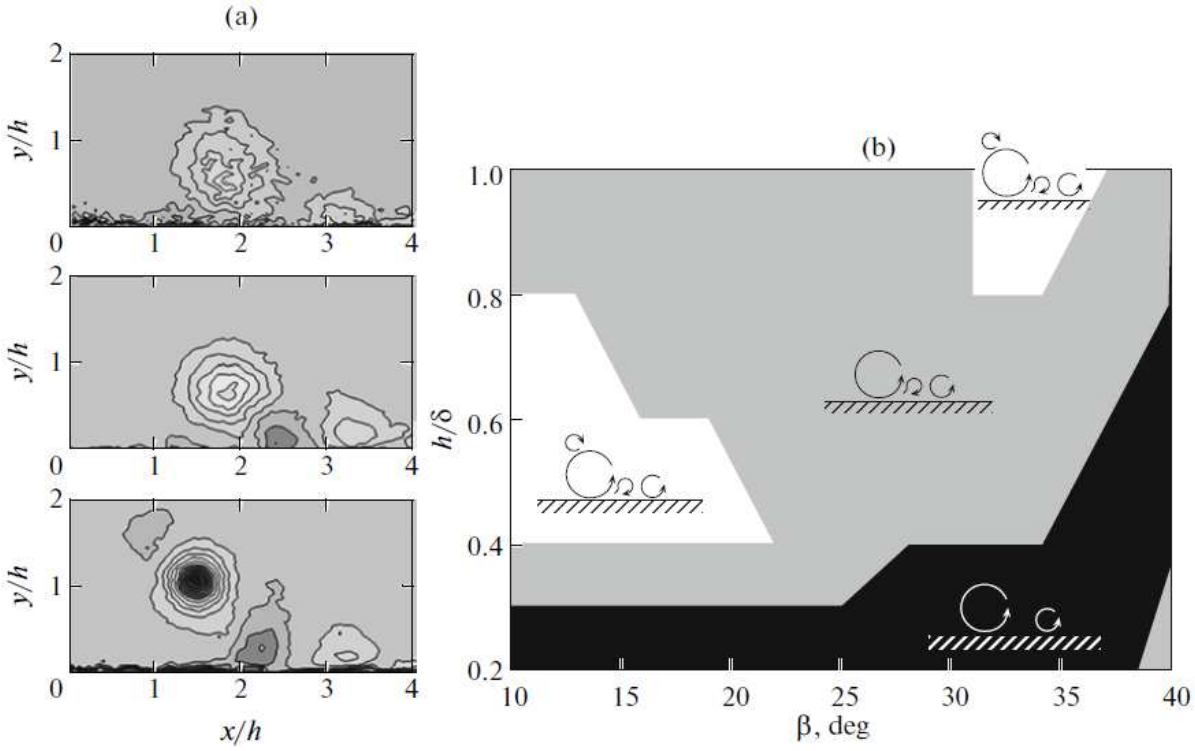

Figure 3: Regimes of the different wake vortex structures produced behind the vane.

REFERENCES

[1] Taylor HD, Research Department Report No. R-4012-3 (Unitged Aircraft Co., East Hartford, 1947).

[2] Velte CM, Hansen MOL and Okulov VL, “J. Fluid Mech.” 619 (2009) pp. 167–177.

[3] Kramer W, Clercx HJH and van Heijst GJF, “Phys. Fluids” 19 (2007), 126603.

[4] Harris DM, Miller VA and Williamson CHK, “Phys. Fluids” 22 (2010), 091106.

[5] Velte CM, Okulov VL and Naumov IV, “Techn. Phys. Letters” 38 (2012), pp. 379-382.

[6] Schmidt JJ, Experimental and numerical investigation of separated flows. PhD thesis, Tehcnical University of Denmark, Kgs. Lyngby (1997).

[7] Harvey JK and Perry FJ, “AIAA J.” 9 (1971) pp. 1659–1660

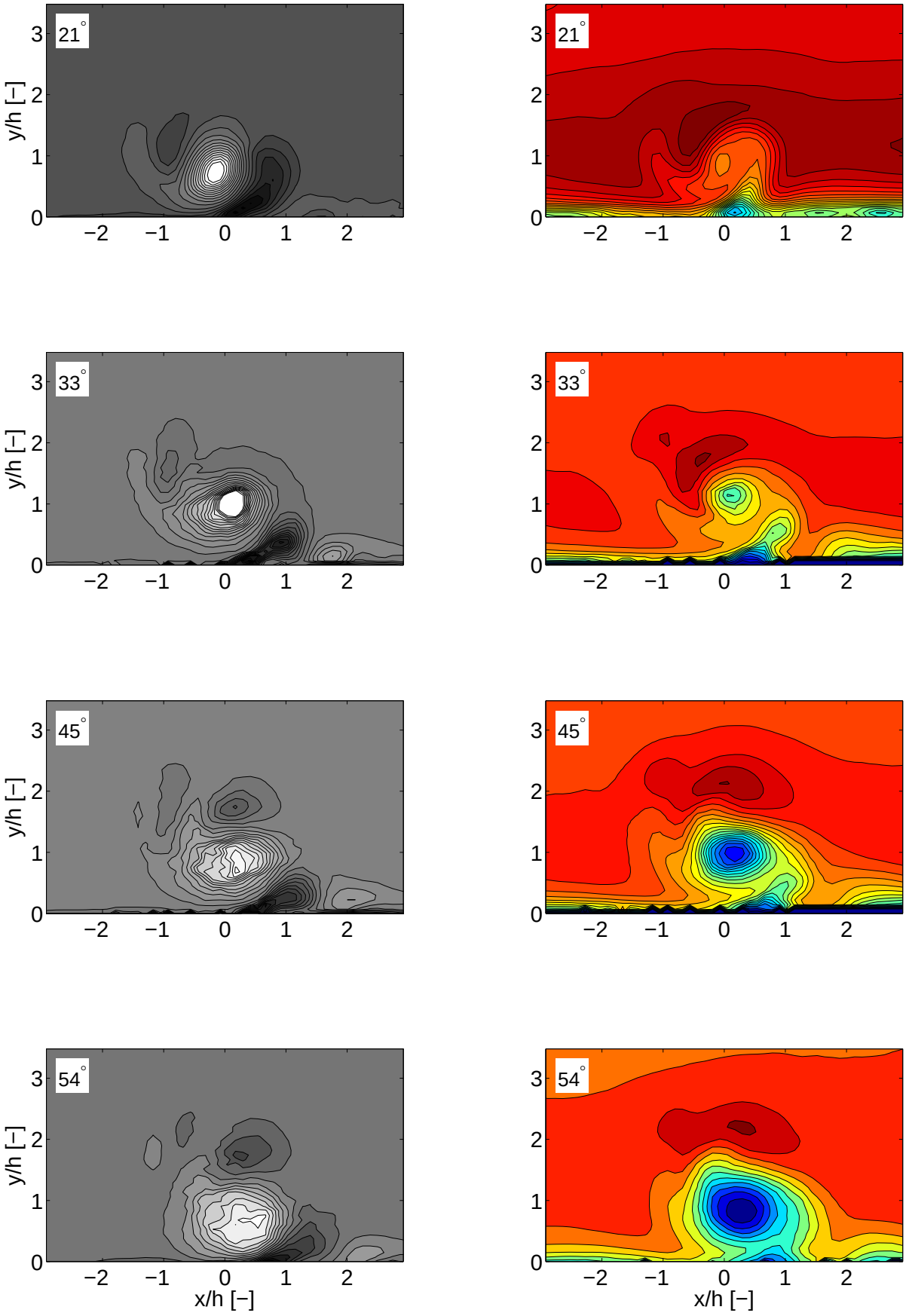

Figure 4: Correlation between streamwise vorticity (left column) and streamwise velocity (right column) in the near wake at $x = 3h$.

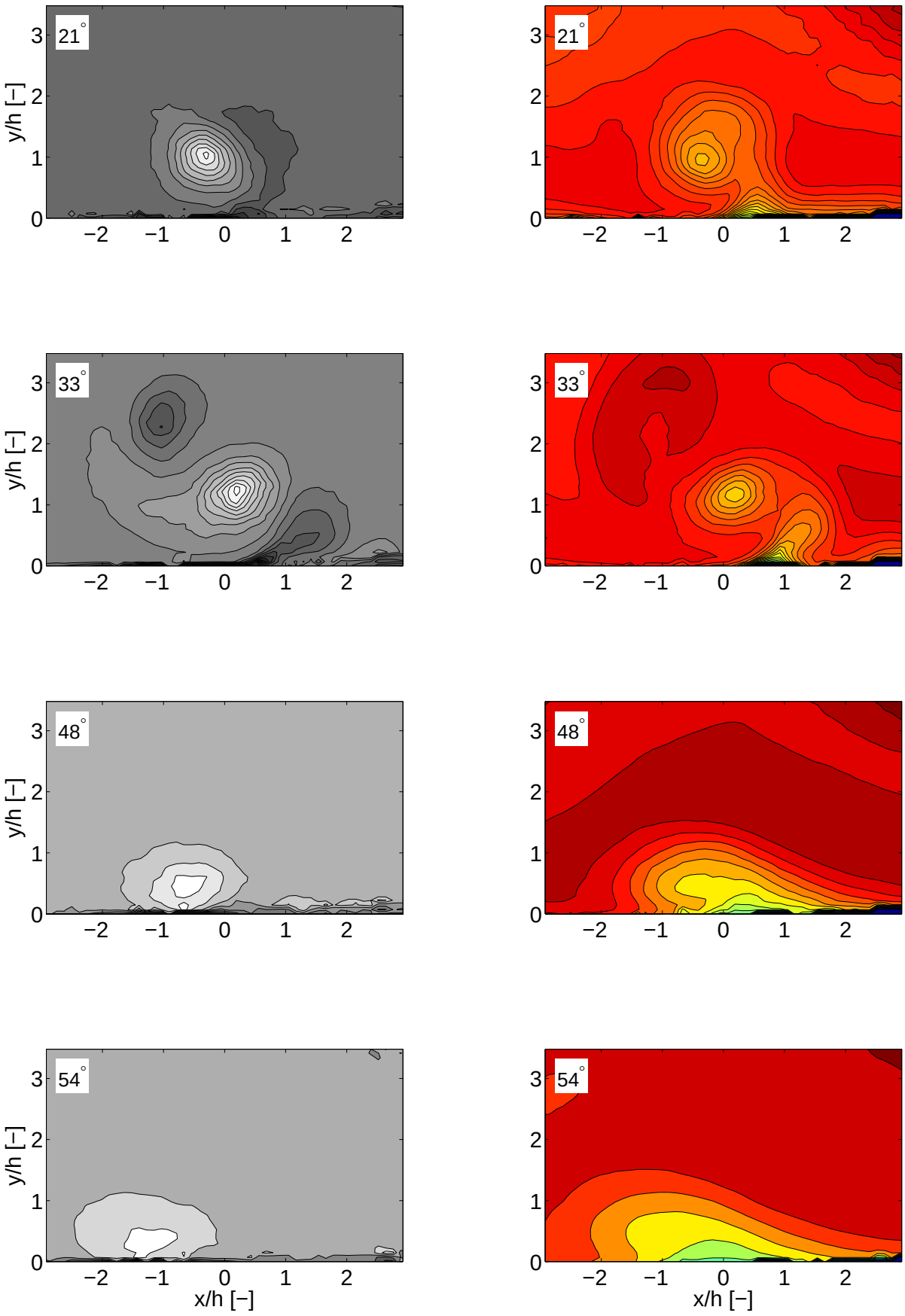

Figure 5: Correlation between streamwise vorticity (left column) and streamwise velocity (right column) in the far wake at $x = 10h$.